Received: 31 October 2021 | Revised: 9 January 2022 | Accepted: 14 January 2022

DOI: 10.1002/er.7702

RESEARCH ARTICLE

INTERNATIONAL JOURNAL OF ENERGY RESEARCH WILEY

Study of radionuclide inventory in nuclear fuel under uncertainties in boron concentration using high-fidelity models

Christian Castagna | **Erez Gilad**

The Unit of Nuclear Engineering, Ben-Gurion University of the Negev, Beer-Sheva, Israel

Correspondence
Erez Gilad, The Unit of Nuclear Engineering, Ben-Gurion University of the Negev, Beer-Sheva 8410501, Israel.
Email: gilade@bgu.ac.il

Funding information
Israeli Ministry of Energy, Grant/Award Number: 219-11-115

Summary

Uncertainties in the critical boron concentration during reactor burnup calculations strongly affect the spectrum, thus propagating to the 1-group cross sections and reaction rates used in the Bateman equations and eventually affecting the resulting nuclide densities. These, in turn, alter the calculated critical boron concentration and so on. Usually, the uncertainty due to this nonlinear feedback is overlooked since only final (ie, at the end of the cycle) radionuclide densities are considered for fuel and waste management. However, for source term analysis, an accurate estimation of the core's radionuclide inventory is required at any time during the irradiation cycle. This paper presents an in-depth uncertainty analysis on the nuclide inventory calculations by considering the nonlinear feedback due to deviation from the critical boron concentration during calculation. In particular, the physical characterization of the interrelated effects among spectrum, cross-sections, reaction rates, and boron concentration are highlighted. The results indicate that deviation from the critical boron concentration during calculation may lead to significant discrepancies in nuclide densities during the irradiation cycle, which tends to decrease towards the end of the cycle. The physical processes underlying this behaviour are studied in depth using a high-fidelity model and the Monte Carlo transport calculations. The methodology presented in this study may be used for systematic uncertainty and sensitivity analysis.

KEYWORDS

boron concentration, burnup, high-fidelity model, Monte Carlo, NuScale

1 | INTRODUCTION

In nuclear engineering, burnup analysis studies the change of composition of the nuclear fuel during the reactor operation. Two main applications in safety analysis are the burnup credit and the source term evaluation. The former relates to the reactivity credit of the discharged spent fuel concerning the safety requirement. A conservative approach in burnup credit aims at overestimating the reactivity of the fuel during the cycle by

simplified and stringent assumptions in the modeling. The model parameters affected by a conservative approach include, for example, the definition of the axial burnup profile, irradiation parameters, control rod worth, boron concentration, and moderator and fuel temperatures. For more details, the reader is referred to Ref. 1.

The source term evaluation allows assessing the radiological impact of an accidental radioactivity release to the environment. The source term is characterized by considering the fuel composition (ie, the radionuclide inventory in the core) at the time of the accident, and the type of the accident.

In the reality of a highly competitive energy market, strict nuclear regulators, and continuously tightened safety requirements, a conservative approach may be impractical and unrealistic. Indeed, a conservative approach in burnup credit dramatically affects the fuel and waste management of the reactor, inflicting significant operation and economic implications.[2]

In the past decade, a favorable alternative has been developed to achieve better modeling accuracy, the so-called "best estimate" methodology, which relies on high-fidelity models, employing coupled Monte Carlo neutron transport calculations, burnup calculation, and thermal-mechanics and thermal-hydraulics codes.[3-6] To validate these approaches, benchmark analysis with experimental data[4] is of primary importance.

The adoption of high-fidelity models in burnup analysis is essential for reliable and accurate assessment of the three main reactivity control mechanisms: soluble absorbers, burnable poisons, and control rods. These absorbers strongly interact with the spectrum and power distribution, affecting the local and global fuel burnup distribution and nuclide densities. The operators manually change the soluble boron concentration during normal operation to control the core's reactivity. Thanks to its high thermal capture cross section, the soluble boron is employed in many Light Water Reactor (LWR) designs. It is dissolved in water in the form of boric acid (H_3BO_3), and its concentration can be adjusted during the reactor operation by filtering it out of the primary coolant. For a given core configuration, the boron concentration required to reach criticality is called the *critical boron concentration* (CBC).

Lattice codes used in the industry incorporate the CBC calculation with a two-step procedure.[6] Here, the first step consists of the condensation and homogenization of the cross sections and diffusion coefficients. Respectively, it means that they are discretized in energy and space to have a few group energy representations in a coarse mesh at the full core level. This procedure is carried out by obtaining a good estimation of the neutron flux from the solution of the neutron transport equation at the pin cell/fuel assembly level. The second step consists of solving the full core problem through nodalization methods. The neutron flux is obtained by solving the diffusion equation with the cross-sections and diffusion coefficients calculated previously, in the full core geometry discretized into homogenized regions (nodes). Differently, Monte Carlo codes directly solve the neutron transport problem on a full core level. In these codes, the adoption of a priori calculations of the CBC has gained increasing attention in the last decade, facilitated by the increase in the availability of computing power and advanced reactor analysis codes. For example, code validations have been carried out with the typical benchmark problems, that is, VERA[7] and BEAVRS,[8] and with the experimental data of other facilities.[9]

The boron concentration dictates the rate of thermal neutron captures in the boron, which hardens the spectrum. The spectrum hardening (or softening) affects the 1-group cross sections and the reaction rates used to solve the Bateman equations.[10] This, eventually, influences the resulting nuclide densities in the fuel and feeds back on the CBC during the cycle.

In burnup credit calculations, the accurate evaluation of CBC during the irradiation cycle is unnecessary since it can be substituted by some constant value representing an average Fixed Boron Concentration (FBC), as reported in the OECD/NEA state-of-the-art report from 2011.[11] Interestingly, this report states that the differences in nuclide densities at the End Of Cycle (EOC) between CBC and FBC are negligible. Furthermore, suppose a conservative approach is adopted for safety analysis. In that case, it is possible to consider the radionuclide inventory at EOC as the reference for the source term calculation throughout the entire cycle. In this approach, an underestimation of the source term is avoided. However, the overestimation bears its operational and economic cost.[2] For the "best estimate" source term analysis, it is crucial to perform accurate evaluations of the radionuclide inventory throughout the cycle, so an accurate estimation of the source term can be obtained at any time during the cycle.

The lack of a systematic evaluation of the effects of boron concentration on radioisotope inventory *throughout the irradiation cycle* in the OECD/NEA state of the art report from 2011[11] has motivated this work. Eventually, this issue directly affects the source term evaluation and the subsequent severe accident analysis.

This paper aims at providing a novel view and deeper physical insight into the numerical consequences of deviation from CBC during the fuel burnup. The research objectives are achieved by a systematic study using a high-fidelity Monte Carlo model. The consequences to the spectrum, 1-group cross sections, reaction rates, and nuclide densities are analyzed and explained. To the best

of the authors' knowledge, a detailed analysis of these nonlinear feedbacks for radionuclide inventory calculation using a high-fidelity model has not been performed yet. More specifically, the objective of this paper is to quantify the error on the nuclide inventory throughout the burnup cycle due to deviation from CBC.

The case study is a three-dimensional fuel cell, simulated with the Serpent Monte Carlo code.[12] The model is based on the design parameters of the NuScale equilibrium core and cycle[13] and is representative of the central fuel pin of the central fuel assembly in the NuScale core with appropriate dimensions and average enrichment and burnable poison concentrations.

This reactor design, which enjoyed much attention in the nuclear community in recent years, is chosen for analysis because it is new and thanks to its potential for scalability and economic competitiveness.[14] The NuScale design incorporates efficient passive safety systems and is resilient to various accidents due to natural causes, for example, earthquakes and tsunamis.[15] However, core damage due to hostile military actions or terror attacks, for example, explosive warhead hit or penetration, may (and in some cases should) also be considered. This scenario constitutes additional motivation for this study, where accurate knowledge of the nuclide inventory in the core during the irradiation cycle will allow the derivation of an accurate source term.

This study applies the research methodology to a representative three-dimensional pin cell as the first step towards full core calculation. At this stage, the focus is on the physical understanding of the nonlinear feedback due to deviation from CBC.

The paper is organized as follows. Section 2 describes the research methodology, including the theoretical background, the computational tools, and the pin cell model used as a case study. Section 3 presents the results and their analyses, and Section 4 presents the conclusions.

2 | METHODOLOGY

2.1 | The burnup equations

In burnup analysis, the Bateman equations are a set of phenomenological balance equations describing the production-destruction rates of the nuclei in a given region of the core. The Bateman equations constitute a system of coupled nonlinear ordinary differential equations,

$$\frac{dN_i}{dt}=\sum_{j\neq i}^{K}\left(f_{ij}\lambda_j+\sigma_{ij}\phi\right)N_j-\left(\lambda_i+\phi\sigma^i_{abs.}\right)N_i,\quad i=1,\ldots,K, \tag{1}$$

where N_i and λ_i are the density and the decay constant of the ith isotope, ϕ, σ_{ij} and f_{ij} are the 1-group neutron flux, the 1-group microscopic cross section for the transmutation of isotope j to isotope i, and the decay fraction that generates the ith isotope from the jth isotope, respectively, and K is the total number of isotopes considered in the burnup calculations. $\sigma^i_{\text{abs.}}$ is the absorption cross section of the ith $i$thisotope. For completeness, the Bateman set of equations is accompanied by a complementary set of initial conditions $N_i(0)=N_0$.

In this notation, the nonlinearity is implicit, but one should recall that $\phi=\phi(N_i(t),t)$ through the neutron transport equation and that $\sigma=\sigma(\phi)=\sigma(\phi(N_i))$ through the usage of the spectrum in the collapse process to the 1-group cross sections. Nonetheless, separation of time scales and proper spatial mesh enable to employ quasi-static approaches in solving these equations.

The burnup equations are usually represented and solved in the following matrix form[16]:

$$\dot{\underline{n}}=\underline{\underline{A}}\cdot\underline{n},\quad \underline{n}_0=\underline{n}(0), \tag{2}$$

where $\underline{n}$ is the nuclide density vector, $\underline{\underline{A}}$ is the $K\times K$ burnup matrix of elements a_{ij}, corresponding to the sum of the radioactive decays $\lambda_{ij}=f_{ij}\lambda_j$ and the product between the 1-group cross section σ_{ij} and 1-group flux ϕ,

$$a_{ij}=\sigma_{ij}\cdot\phi_{1g}+\lambda_{ij}. \tag{3}$$

In particular, the diagonal elements a_{ii} are the destruction rates corresponding to $-\sigma^{\text{abs.}}_i\phi-\lambda_i$ and are negative and correspond to the absorption rates of the ith nuclide. To distinguish between the decay and the transmutation reaction contributions, $\underline{\underline{A}}$ and a_{ij} can be split as follows:

$$\underline{\underline{A}}=\underline{\underline{R}}+\underline{\underline{D}},\quad a_{ij}=r_{ij}+d_{ij}, \tag{4}$$

where $\underline{\underline{R}}$ and $\underline{\underline{D}}$ are the reaction and the decay matrices, respectively, with entries r_{ij} and d_{ij}, respectively.

The system of burnup equations can be solved by various numerical methods.[17] The core is usually discretized into numerous different volumes (voxels). In each voxel, the 1-group cross sections are computed by collapsing the energy-dependent microscopic cross sections using the neutron spectrum $\phi(E)$ (in the voxel) as a weighting function,[18]

$$\sigma=\frac{\int_0^\infty dE\sigma(E)\phi(E)}{\int_0^\infty dE\phi(E)}. \tag{5}$$

Depending on the user choice, the neutron flux is recalculated at selected time steps[19] and tallied in several energy groups and different voxels in the core.

2.2 | Nonlinear CBC feedback mechanism

As stated in the introduction, boron is used as a reactivity control mechanism in most LWRs. As the core's reactivity decreases over time due to fuel depletion, the boron concentration is adjusted (ie, reduced) accordingly to compensate for the decreasing reactivity. The presence of boron in the core hardens the spectrum due to its high capture cross section of thermal neutrons. Thus, as the boron concentration is reduced during the irradiation cycle, the spectrum is expected to soften with respect to the initial one.

The nonlinear mechanism by which errors in the boron concentration propagate through the calculation and feedback on the critical boron concentration is illustrated schematically in Figure 1. From a modeling perspective, at any time during the cycle, the determination of the boron concentration (whether CBC, FBC, or else) influences, in different ways, the spectrum. This affects the computation of the 1-group cross sections used to solve the Bateman equations in each voxel. The 1-group fission cross sections are also affected by variations of the 1-group flux since they are normalized with respect to the nominal power to conserve the total fission rate.

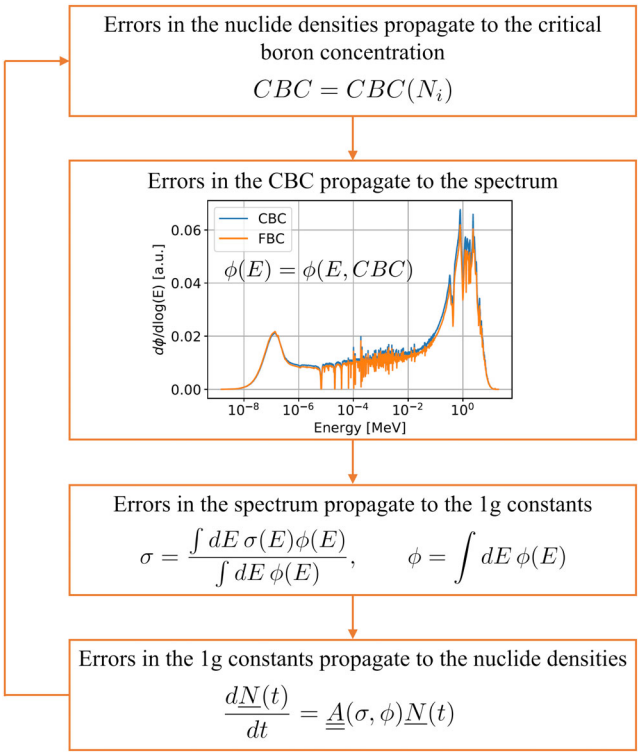

FIGURE 1 Schematic illustration of the s feedback mechanism by which variations in boron concentration affect nuclei density and vice versa. The spectrum shown (in lethargic scale) was obtained by Monte Carlo transport calculations of fresh fuel with critical and fixed boron

2.3 | The criticality iteration method

Some methods to calculate the CBC have been developed for Monte Carlo models.[7,20] In this study, the criticality iteration method is adopted, which is implemented in the Serpent Monte Carlo code.[12] In this method, the neutron balance equation is written in the following form,

$$\frac{1}{k}P_{\text{fiss}} + P_{n\times n} = L_{\text{leak}} + L_{a,B}^{\text{crit}} + L_{a,\text{nucs}}, \tag{6}$$

where k is the criticality eigenvalue, P_{fiss} and $P_{n\times n}$ are the fission and scattering production terms, respectively, L_{leak} is the leakage term, $L_{a,B}^{\text{crit}}$ represents the losses due to absorption in the boron, and $L_{a,\text{nucs}}$ represents the losses due to absorption in other nuclides excluding boron.

At the start of the calculation, a default value of the boron concentration is set n_B^{def}, by obtaining $L_{a,B}^{\text{def}}$. The critical boron concentration n_B^{crit} results by considering a linear dependence between the atomic densities of the boron nuclei and the boron capture rate. So the default boron concentration is scaled by a factor g at every burnup step, where

$$g = \frac{L_{a,B}^{\text{crit}}}{L_{a,B}^{\text{def}}} = \frac{n_B^{\text{crit}}}{n_B^{\text{def}}}. \tag{7}$$

2.4 | Benchmark problem

The critical boron iteration method is applied to a benchmark problem in the form of the central fuel cell of the central Fuel Assembly (FA) of a NuScale core,[13] which reproduces the conditions of an infinite lattice adequately. The model geometry, materials, and temperature are detailed in Table 1.

Reflective boundary conditions are applied in the radial direction. Two axial reflectors are modeled above and below the active zone by 30 cm (each) of stainless steel and water mixture (80% and 20% volumetric fraction of stainless steel and water, respectively). At the reflector ends, vacuum boundary conditions are set. The fuel and coolant temperatures are set uniformly to 900 and 600 K

TABLE 1 Design parameters of the NuScale fuel cell. The power of the single pin is calculated by multiplying the average pin power (16.5 kW) with the relative power distribution of the central FA (1.1) and fuel pin (1.2)

Parameter	Value	Parameter	Value
Height	200 cm	Fuel	UO_2
Internal radius	0.4058 cm	Enrichment	2.6%
External radius	0.4140 cm	Power	22 kW
Cladding radius	0.4763 cm	T_{fuel}	900 K
Pitch	1.25984 cm	$T_{coolant}$	600 K

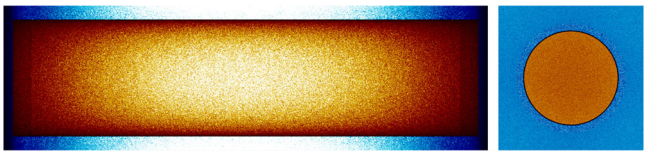

FIGURE 2 Axial and radial plot of fission power (red/yellow) and thermal flux (blue) distributions, generated by neutron transport calculations in Serpent

values, respectively. Figure 2 shows the geometry with fission power and thermal flux distributions generated by Serpent.

Two burnup histories are considered to evaluate the nonlinear feedback effect of boron concentrations on nuclei density. The first one, with CBC, was calculated throughout the cycle using the criticality iteration method. The second one, with FBC at 810 ppm, was obtained by averaging the previous CBC simulation's boron concentration.

The burnup cycle length is 750 days (~2 years), similar to that of the NuScale core, with initial burnup steps at 0.1, 0.5, 1, 2, 7, 15, and 30 days, and continue with steps of 30 days until EOC. The fuel pin is divided into 10 axial equivolume burnup regions. We adopt the Stochastic Implicit Euler (SIE) method, a burnup scheme that performs several inner iterations to under-relax the flux to stabilize the burnup solution. We employ this scheme to prevent the numerical instabilities due to flux/xenon oscillations, typical of Monte Carlo burnup calculation codes.[21]

The number of neutron histories is 2×10^7 with 20 inner iterations at each burnup step, allowing a statistical uncertainty of around 30 pcm on k_{eff}. Regarding the nuclear data, the cross-section library ENDF/B-VII[22] is employed. The neutron spectrum is tallied with the energy discretization of the ECCO1968 group structure.[23] In order to obtain and report reliable results, several realizations are performed and the averages are considered. A total of eight independent realizations of an identical input are executed for the CBC and FBC cases, obtaining a relative uncertainty of less than 0.4% on the averaged densities of all nuclei. These are taken as the reference results.

2.5 | Methodological approach to evaluate CBC effects

The impact of boron concentration is quantified by defining a percentage error $e(x)[\%]$ for all the physical quantities y under consideration:

$$e(x)[\%] = \frac{y_{\text{crit.}}(x) - y_{\text{fix}}(x)}{y_{\text{fix}}(x)} \times 100, \quad x \in [E, t], \tag{8}$$

where x can be either the energy E or the time t, depending on what is studied, the spectrum or the densities. The error analysis is performed in three steps, following the logical flow of the explanatory scheme in Figure 1.

1. Analysis of the errors associated with spectrum variations.
2. Propagation of spectral errors to the 1-group cross sections, flux, and reaction rates.
3. Analysis of the impact on the density, activity, and radiotoxicity of the nuclei of interest in source term analysis.

The next section discusses the results concerning this scheme.

3 | RESULTS

3.1 | Spectral uncertainty analysis

First, it is essential to verify that the criticality density iteration method simulates the boron variation correctly over time. Other reactivity control mechanisms are not considered, that is, control rods and burnable poisons thus the CBC compensates for their effects. For this reason, the CBC values are scaled by a factor of 0.51, corresponding to their relative contribution concerning all other control systems in a typical PWR.[24] The shape of the boron letdown, shown in Figure 3, is well reproduced (left) and the reactivity remains zero throughout the cycle (right). Moreover, despite the approximation of the single fuel cell model, the values are in good agreement with those obtained by the full core analysis of NuScale,[13] where the concentration is around 1200 ppm at BOC and 600 ppm at the Middle of Cycle MOC. As expected, the

reactivity decreases over time in the simulations with FBC (at 600 ppm).

The normalized spectrum of the two sets of simulations (FBC and CBC) is compared at the BOC and the EOC, as shown in Figure 4. Compared to the FBC, the CBC spectrum becomes softer over time due to decreased boron concentration. This trend is quantified by the relative difference between the CBC and FBC boron spectra, $e(E)[\%] = [y_{\text{crit}}(E) - y_{\text{fix}}(E)]/y_{\text{fix}}(E) \times 100$, where $y(E) \equiv d\phi(E)/d\log(E)$. The relative difference is shown in the lower panels of Figure 4. Initially, the difference is negative in the thermal region, with values around −5%, and positive in the epithermal and fast regions, reaching 10% to 11% for energies above 10^{-5} MeV. This indicates a harder spectrum in the critical boron case. At the end of the core's life, the trend is reversed.

To study the spectrum behaviour along the cycle, the spectrum is divided into thermal, epithermal, and fast regions, according to the energy ranges [<1 eV], [1 eV-100 keV], and [100 keV-20 MeV], respectively. The error in the FBC spectra is quantified as a measure for the average difference between the spectra for each energy region for each time step $e_{\phi_E}(t)[\%] \equiv \int_{\Delta E}[y_{\text{crit}}(E,t) - y_{\text{fix}}(E,t)]dE / \int_{\Delta E} y_{\text{fix}}(E,t)dE \times 100$ and is reported in Figure 5. The thermal spectrum error is negative at around −2% at BOC and increases over time, reaching around 3% at EOC. This trend reflects (and quantifies) the softening of the CBC spectrum concerning the FBC spectrum during the cycle. For the same reason, the epithermal and fast spectra trend is reversed, with values between 6% and −4%.

3.2 | Spectral uncertainty propagation to 1-group cross sections

During the burnup analysis, the spectrum errors are propagated into the calculation of the 1-group cross sections used in the Bateman equations (Equations 1-4). The errors in the 1-group microscopic fission cross section $e_{\sigma_{\text{fiss.}}}$ are shown in the left panel of Figure 6 for the most important fissile and fissionable nuclei, that is, ^{235}U, ^{238}U, ^{239}Pu, and ^{241}Pu. The specific isotope is indicated by its atomic mass number. The cross section error for isotope i for reaction r is define as $e^i_{\sigma_r}(t)[\%] = \left[\sigma^i_{r,\text{crit}}(t) - \sigma^i_{r,\text{fix}}(t)\right]/\sigma^i_{r,\text{fix}}(t) \times 100$.

The errors in the 1-group microscopic fission cross section $e_{\sigma_{\text{fiss.}}}$ follows the trend of the *thermal* flux spectral error e_{ϕ_E} for the fissile isotopes (recall Figure 5). This is due to higher values of the fission cross sections at thermal energies that weigh more on the final calculation of 1-group cross section. This trend is expected for a softening spectrum. Note that the errors $e_{\sigma_{\text{fiss.}}}$ change between −8% and +8%, larger than the thermal error in the spectrum e_{ϕ_E}. In the case of ^{238}U, the behaviour is reversed with a lower magnitude (between +1% and −1%) and a trend similar to the *epithermal* and the *fast*-flux spectral error e_{ϕ_E}, since its fission cross section is zero in the thermal energy region and assumes a non-zero value only at the epithermal and fast energy regions.

The errors in the microscopic 1-group capture cross section $e_{\sigma_{\text{capt.}}}$ are shown in the right panel of Figure 6 for ^{135}Xe and ^{149}Sm (major poisons), ^{131}I (a radioactive fission product) and ^{241}Am (a radioactive actinide). Since the radiative capture cross sections for the selected isotopes are higher at the thermal energy region, $e_{\sigma_{\text{capt.}}}$ follows the trend of the *thermal* flux spectral error e_{ϕ_E}. It is important to note that these errors are not negligible, reaching values between −10% and 11% for ^{135}Xe and ^{149}Sm. These isotopes are among the main poisons in the reactor core, and errors in their densities may also impact the reactor's safety analysis report and its operational conditions.

3.3 | Cross-section uncertainty propagation to the flux and reaction rates

The reactor power is constant and identical throughout the numerical simulations for both CBC and FBC cases.

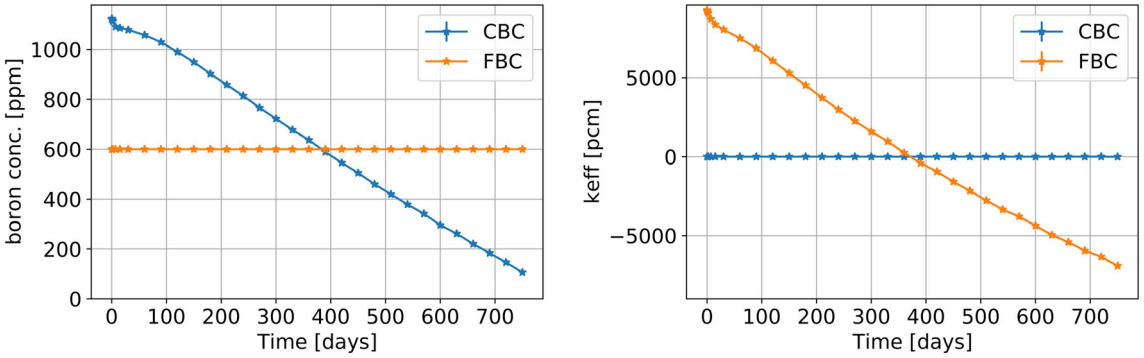

FIGURE 3 Boron concentration (left) and reactivity (right) over time, comparing the case with CBC and FBC

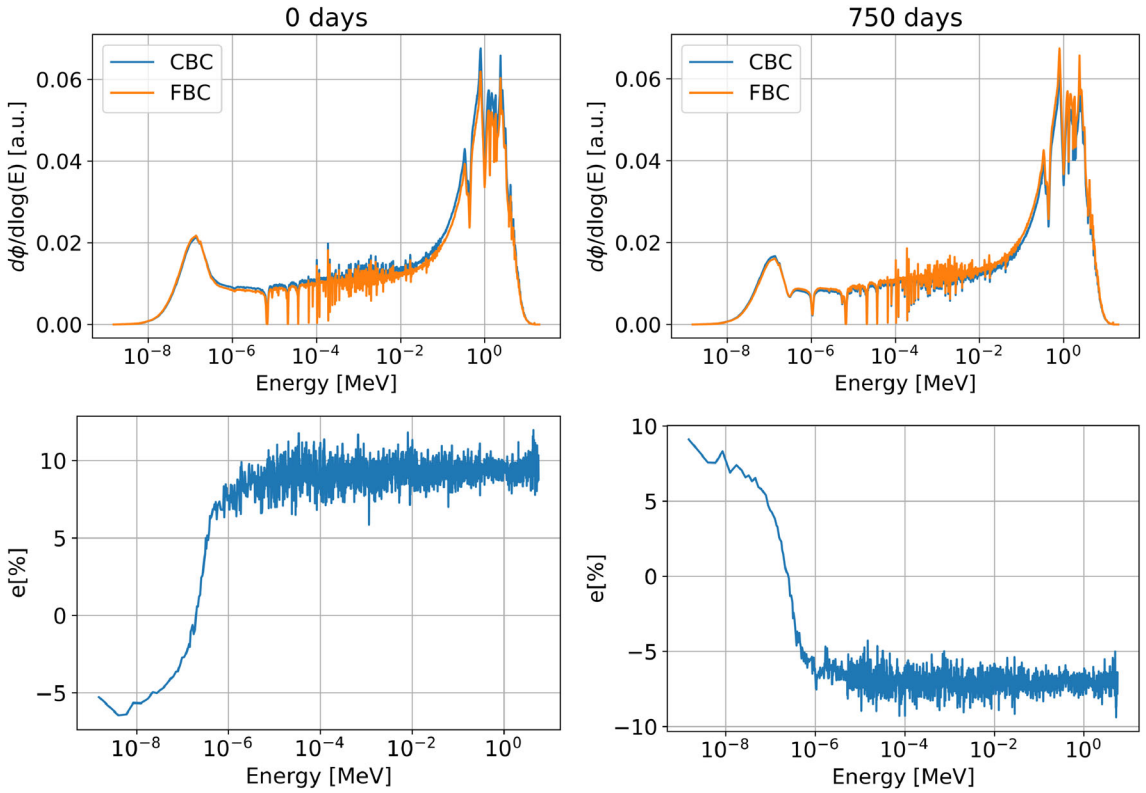

FIGURE 4 Spectra and relative difference for FBC and CBC simulations. The upper panels show the normalized spectrum on the lethargic scale and the lower panels show the relative difference between CBC and FBC spectra. The left and right panels are for BOC and EOC, respectively

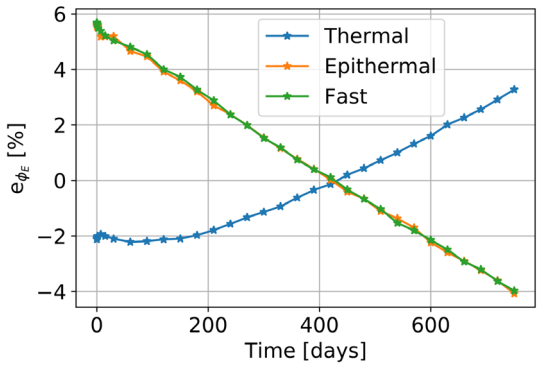

FIGURE 5 Quantification of the error in the FBC spectra with respect to the CBC spectra for each energy region for each time step

The conservation of the total fission rate in the core dictates flux variations such that the variations in the fission cross section ($e_{\sigma_{\text{fiss.}}}$) are compensated. The error in the 1-group flux between FBC and CBC cases during the irradiation cycle is reported in Figure 7, where its values range between 7.5% and −6%. The trend is opposite to that of the error in the fission cross section $e_{\sigma_{\text{fiss.}}}$ of the fissile isotopes, as expected for constant reactor power.

So the opposite trends in the errors in the 1-group fission cross section and the flux yield a constant power which is proportional to $\sigma_f \phi$. However, in the Bateman equations (Equations 1-4), the 1-group flux appears in additional multiplication terms with other (not fission) cross sections. The general form of these terms is $\sigma_{ij}\phi$, which stands for other transmutation reaction rates, for example, radiative capture (n,γ) and inelastic scattering $(n,2n)$. These terms, in general, do not conserve the reaction rates concerning the CBC case. Hence, it follows that both uncertainties, in the 1-group flux e_ϕ and cross sections e_σ, need to be considered for an in-depth study of the boron concentration effect and its associated spectral uncertainty on the resulting nuclide densities.

In particular, it is highly valuable to provide a physical explanation to the error analysis through the cycle and the burnup computational scheme. This is challenging since a single nuclide (Bateman) equation is unique and coupled to other equations, in relation to the reaction rates and decays that involve the specific nuclide under consideration. It is obvious that providing a physical explanation for each isotope (∼1200 of total isotopes) is not possible.

Therefore, only a few representative isotopes are considered in the analysis of uncertainty propagation into the 1-group cross section, that is, ^{131}I, ^{135}Xe, ^{235}U, ^{238}U, ^{239}Pu, and ^{241}Am. The relative errors in cross section e_σ

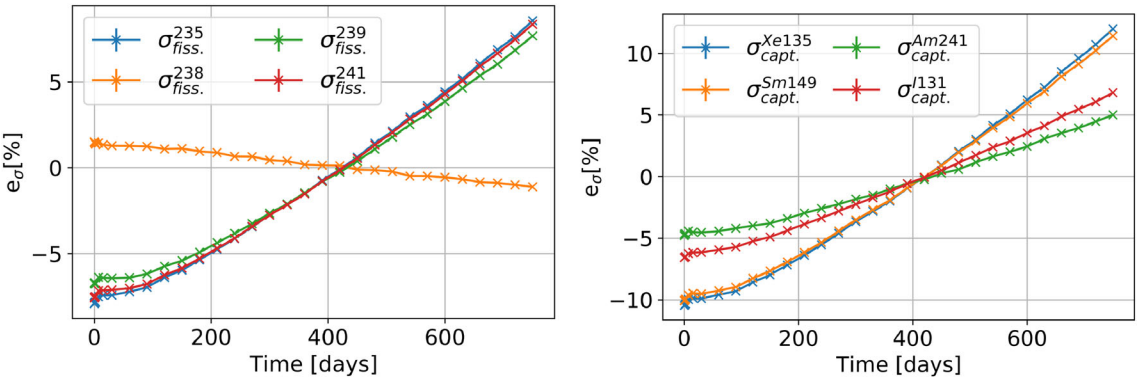

FIGURE 6 Errors in the fission and capture microscopic 1-group cross sections for selected radionuclei

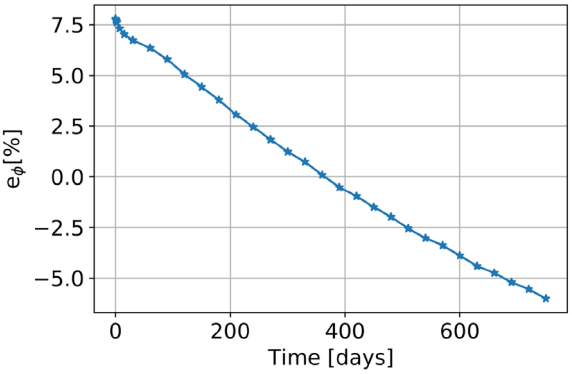

FIGURE 7 The relative error in the 1-group flux e_ϕ between FBC and CBC cases during the irradiation cycle

and reaction rate of destruction $e_{r_{ii}}$, associated with the absorption term $r_{ii} = -\sigma_i^{abs}\phi$ are compared between FBC and CBC cases in Figure 8. In Figure 9, the relative errors in isotope density $e_{dens.}$ are reported for the selected isotopes. The nuclei are indicated by their atomic mass number.

For ^{235}U, the error in the absorption cross section $e_{\sigma^{235}_{abs.}}$, which is dominated by the major contribution of $e_{\sigma^{235}_{fiss.}}$, is compensated by the errors in the flux (see Figure 7), which exhibit an opposite trend. The resulting absolute value of the error in the absorption reaction rate $e_{r^{235}_{ii}}$ is less than 1% throughout most of the cycle. Since the burnup of ^{235}U depends only on the absorption rate (no production terms through decay or transmutation), the small errors in the absorption reaction rate $e_{r^{235}_{ii}}$ lead to negligible errors in the isotope density e^{235}_{dens}.

For ^{238}U, only errors in the absorption reaction rate $e_{r^{238}_{ii}}$ should be considered, similarly to ^{235}U. The error in the flux is much larger (up to 8% difference) than the error in the absorption cross section $e_{\sigma^{238}_{abs.}}$, leading to a significant error in the absorption reaction rate $e_{r^{238}_{ii}}$, which follows the same trend of e_ϕ. Although the relative error in the absorption rate $e_{r^{238}_{ii}}$ is between 7.5% and −5%, the impact on error in the nuclide density e^{238}_{dens} is negligible. This is unique to ^{238}U due to its high nuclide density in the core and its relatively small absolute value of the absorption rate.

Since ^{239}Pu is obtained from the capture of a neutron in a ^{238}U nucleus, the initial positive (and final negative) relative error in the absorption cross section $e_{r^{238}_{ii}}$ is reflected in the relative error of the nuclide density e^{239}_{dens}, which exhibits a similar trend. Additionally, the relative error in the absorption cross section $e_{r^{239}_{ii}}$ is small and negative for the majority of the fuel cycle, contributing to a significant positive e^{239}_{dens}, which ranges between 6% and −2%.

The following expression describes the Xenon density at equilibrium[24]:

$$N^{eq.}_{Xe} = \frac{r^{therm.}_{fiss.}(\lambda_{Xe}+\lambda_I)}{\sigma^{Xe}_{abs.}\phi_{th.}+\lambda_{Xe}} \cong \frac{r_{fiss.}(\lambda_{Xe}+\lambda_I)}{r^{135}_{ii}+\lambda_{Xe}}, \tag{9}$$

where $\phi_{therm.}$ is the thermal flux, $r^{therm.}_{fiss.}$ and $r_{fiss.}$ are the thermal and the total fission rate, respectively, $\sigma^{Xe}_{abs.}$ is the thermal absorption cross section of ^{135}Xe, and λ_{Xe} and λ_I are the decay constants of ^{135}Xe and ^{135}I, respectively.

Since the thermal part of the flux dominates both the total fission and Xenon absorption rates, $r^{th.}_{fiss.}$ is approximated as the (constant) total fission rate $r_{fiss.}$, and $\sigma^{Xe}_{abs.}\phi_{th.} \cong r^{135}_{ii}$. In the first half of the irradiation cycle, $e_{r^{135}_{ii}}$ is negative, that is, lower absorption rate for the CBC case compared to the FBC one, which results in higher values of $N^{eq.}_{Xe}$ and positive $e^{135}_{dens.}$. In the second half of the cycle, the trend is reversed.

The ^{241}Am isotope is generated by the β^- decay of ^{241}Pu, created by neutron capture by ^{240}Pu and ^{239}Pu. As shown in Figure 9, the errors in the density of plutonium isotopes are cumulative, that is, the errors are accumulated by propagating to isotopes with higher atomic numbers. For example, ^{239}Pu is the source for ^{240}Pu

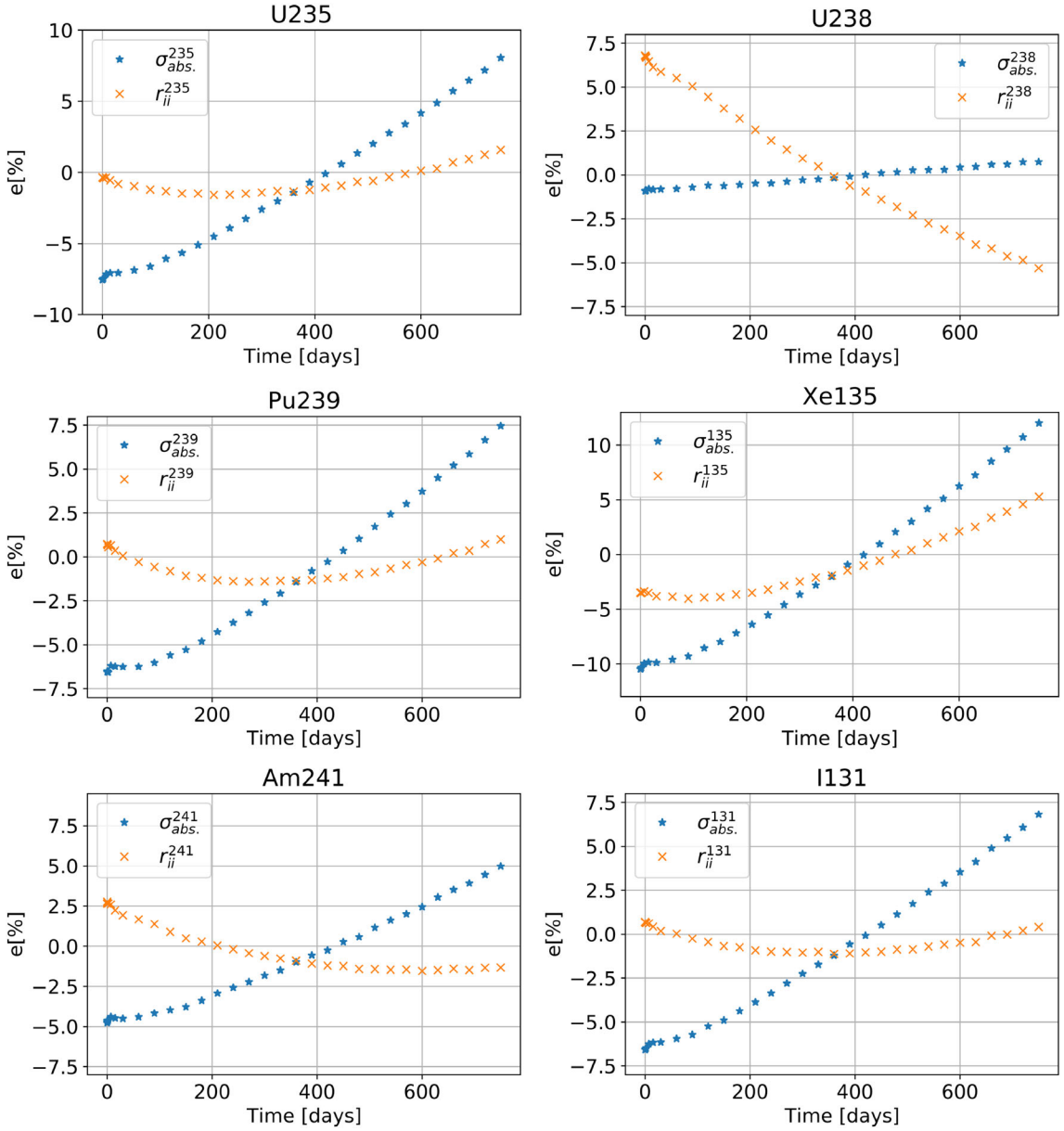

FIGURE 8 The relative errors in absorption cross section $\sigma_{\text{abs.}}$ and reaction rate of destruction r_{ii} between the FBC and CBC cases for selected isotopes selected

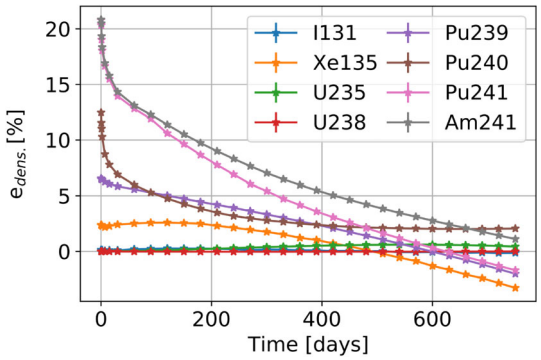

FIGURE 9 The relative error in the nuclide densities between the FBC and CBC cases for several selected isotopes

(by neutron capture), hence errors in ^{239}Pu will be propagated to the density of ^{240}Pu. On the other hand, the density errors of ^{241}Am are the same as ^{241}Pu at the BOC, which is probably due to the small absolute densities of both isotopes. After BOC, the error in ^{241}Am density remains higher than ^{241}Pu, since, as reported in Figure 8, the error in destruction rate of ^{241}Am r_{ii}^{241} decreases over time.

The production of ^{131}I depends on the fission rate, which is the same for the CBC and FBC cases. The destruction rate is mainly due to its decay and the impact of the capture on its density is negligible. For these reasons, e_{dens}^{131} is not significant. Many other fission products

(direct or indirect) exhibit similar behaviour due to similar reasons, for example, Ba, Sr, La, and Mo.

3.4 | Uncertainty analysis on source term isotopes

The source term analysis is based on the characterization of the radioactive material contained in the fuel to evaluate its dispersion due to a reactor accident. The radionuclide inventory of interest was revised over the years by the US NRC until the current version in the report from 1995 NUREG-1465,[25] shown in Table 2.

TABLE 2 NUREG-1465 Revised source term radionulide inventory[25]

Group	Elements
Noble gases	Xe, Kr
Halogens	I, Br
Alkali metals	Cs, Rb
Barium and Strontium	Ba, Sr
Noble metals	Ru, Rh, Pd, Mp, Tc, Co
Lanthanides	La, Zr, Nd, Eu, Nb, Pm, Pr, Sm, Y
Tellurium group	Te, Sb, Se
Cerium group	Ce, Pu, Np

Note that the density of these elements is only an indication in safety analysis, for which it is more important to consider their activity. Indeed, also isotopes in small relative quantities can contribute significantly to the total radioactivity of the single element.

From the radionuclides specified in Table 2, those with density and activity errors higher than 0.5% are shown in Figure 10. The elements are grouped in four panels for fission products (top) and actinides (bottom), and for density (left) and activity (right) errors. The americium is also included since it is considered in other reports and radiological analyses.[26]

The relative errors in elements' activity $e_{\text{act.}}$ are higher than the relative errors in their density $e_{\text{dens.}}$. All the errors decrease over time; even though each variation can be explained by the physical interpretation of the Bateman equations, as done in the previous section, the general trend follows the flux errors. In addition to americium, significant errors are also exhibited by cobalt and neptunium, the last one particularly significant since it contributes about 50% to the total actinides activity.

The results suggest that an accurate (best estimate) evaluation of the isotopic inventory at any time during the cycle can be performed by employing CBC, avoiding significant errors. Indeed, the magnitude of density errors

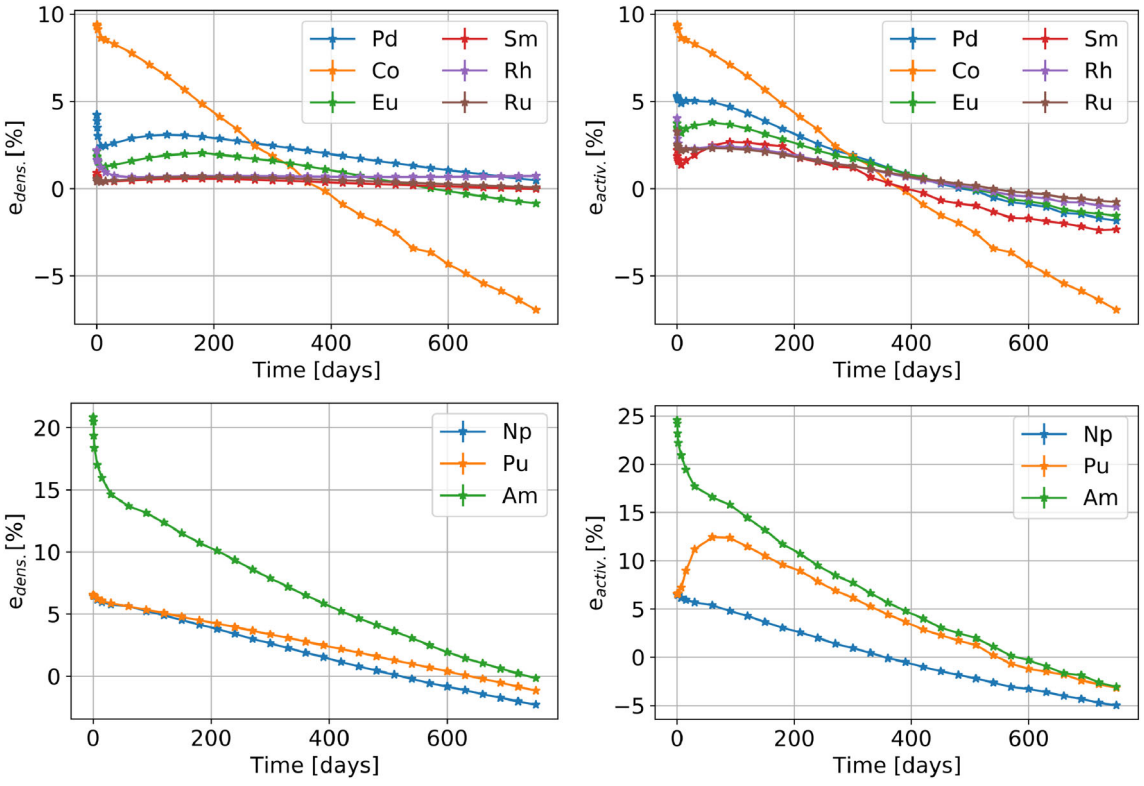

FIGURE 10 Errors in nuclide densities (left) and activities (right) for selected fission products (top) and actinides (bottom)

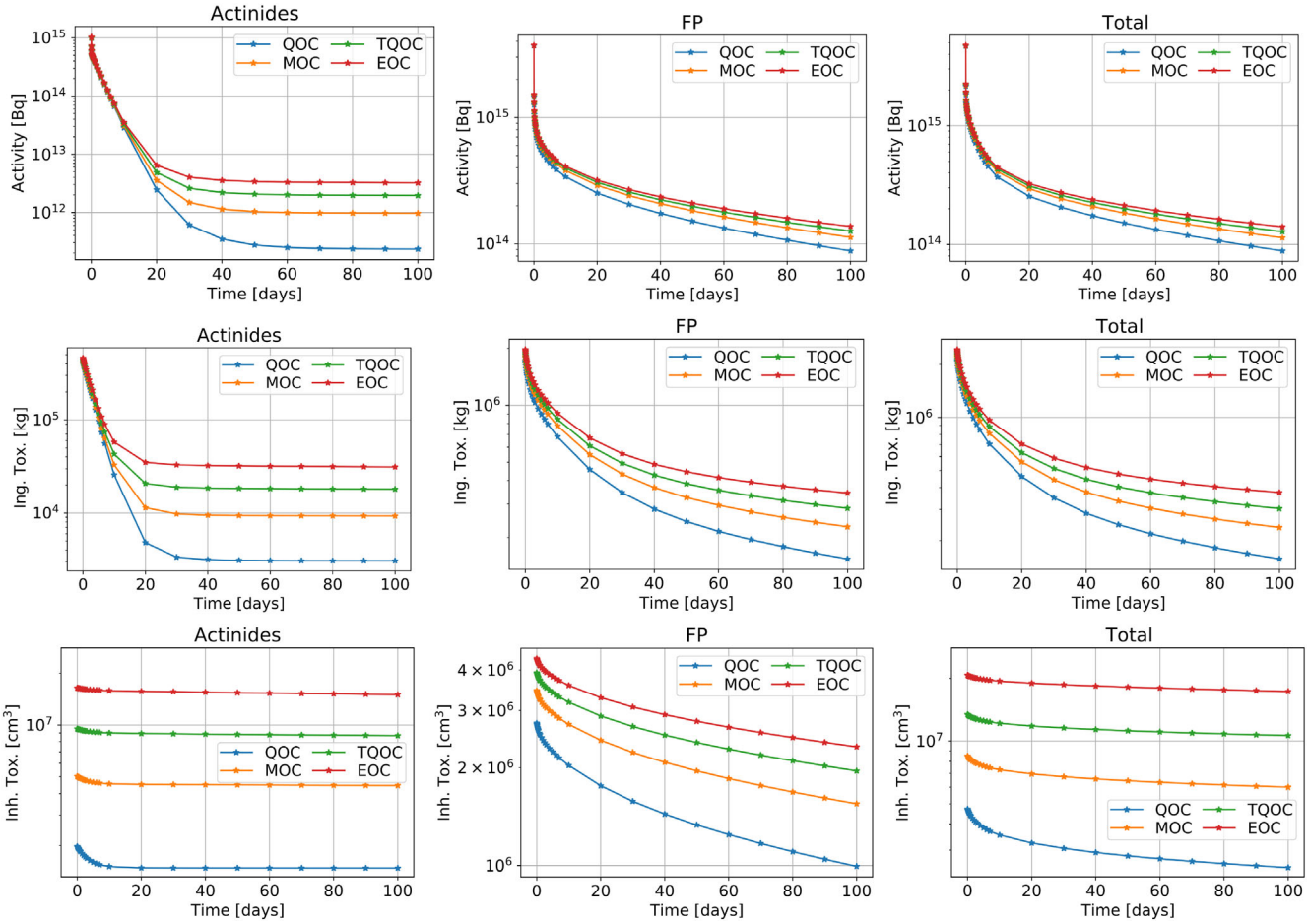

FIGURE 11 Activity, ingestion, and inhalation radiotoxicity for actinide, FP, and total group, after reactor shutdown at different times

$e_{\text{dens.}}$ reaches high values considering the uncertainties from other input parameters, enrichment, temperatures, and sample burnup, in spent fuel analysis.[11] Furthermore, $e_{\text{dens.}}$ is compatible with the values of a typical uncertainty propagation of the nuclear data in LWR fuel, as described in[27] for ^{239}Pu (1%-2%), ^{237}Np (4%-15%), and ^{241}Am (4%-15%).

3.4.1 | Error in activity and toxicity after shutdown during the cycle

In source term analysis, it is also important to evaluate the activity of the radionuclides after reactor shutdown, whether planned or emergency. To obtain an indicative impact of activity errors in this situation, decay calculations were performed for CBC and FBC cases, simulating the reactor shutdown at Quarter of Cycle (QOC), Middle Of Cycle (MOC), Three Quarter Of Cycle (TQOC) and EOC. In this procedure, the reactor power is set to zero at the specific time and the decay is calculated for additional 100 days using the following finer time steps in days: 0.021, 0.042, 0.1, 0.2, 0.3, 0.4, 0.5, 0.8, 1.0, 1.5, 2.0, 2.5, 3, 4, 5, 6, 7, 10, 20, 30, 40, 50, 60, 70, 80, 90, 100.

In addition to the radioactivity, the inhalation and ingestion toxicity errors are also analyzed. They correspond to the air mass (inhalation) and water volume (ingestion) necessary to dilute the radionuclides to permitted concentration levels, to prevent damage to the human body.

The nuclide elements are grouped into Fission Products (FP) and actinides. For the sake of completeness, their activity and radiotoxicity are shown in Figure 11 with the CBC, where these quantities have the typical exponential decrease over time due to radioactive decay.

The relative errors between CBC and FBC if the FP group is negligible, with values under 0.2%. The situation is different for the actinide group, where the errors reach ∼5%, as reported in Figure 12. A decrease if the errors is exhibited from positive at QOC to negative at EOC, reflecting the decrease of $e_{\text{dens.}}$ discussed before.

Notice that the errors at EOC are negative and in the order of 1% to 5% for activity and ingestion radiotoxicity. For this reason, the validity of the assumption in,[11] that

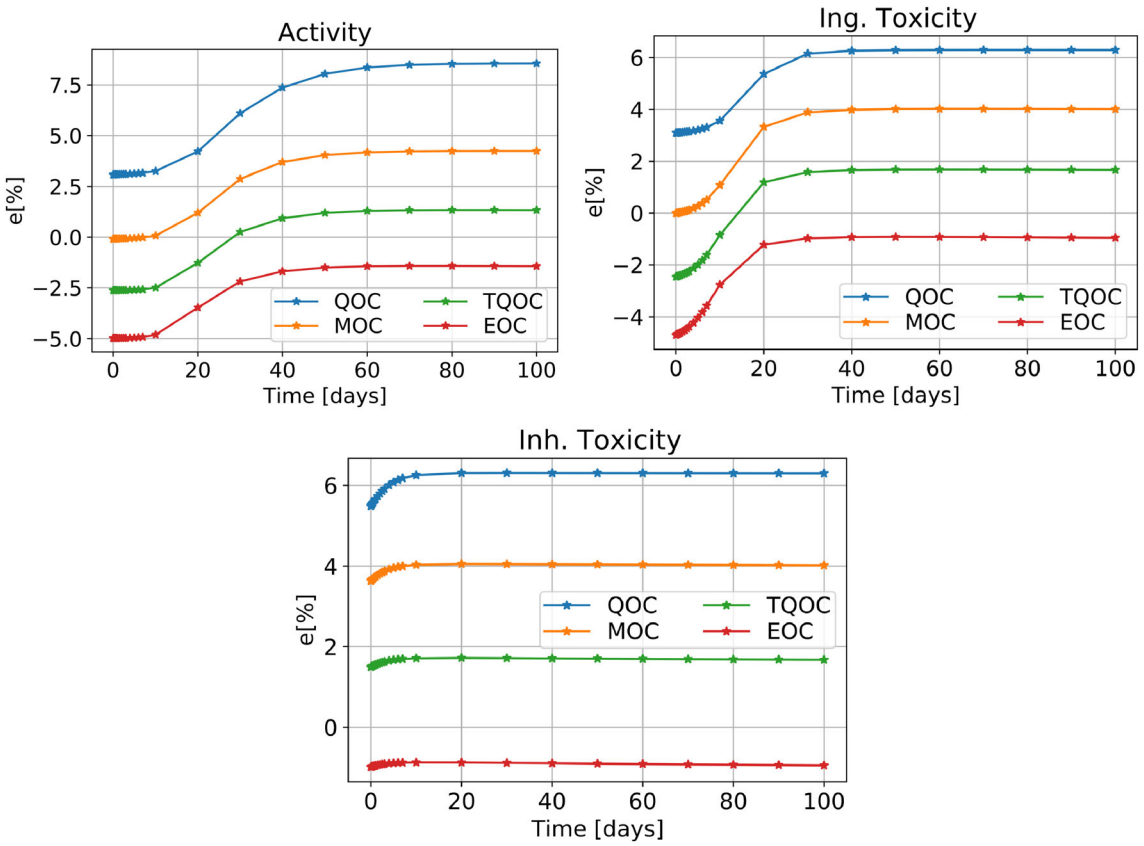

FIGURE 12 Errors on activity, ingestion, and inhalation toxicity, for the actinide group after the shutdown at different times

is, burnup analysis with average FBC and CBC are equivalent in burnup credit, maybe not be generally valid since it depends on the target accuracy of the calculation.

In source term analysis, in addition to the considerations made in the previous section, it is important to note that the errors may become more significant by considering their propagation to estimate the radionuclide release in-gap, in-vessel, ex-vessel, and late in-vessel.[28]

4 | CONCLUSIONS

This work presents a detailed physical analysis of the errors in isotopic inventory calculations due to a departure from critical boron concentration during calculation. The model used is a simplified fuel pin cell with critical and fixed (average) boron concentrations, and the flux and burnup solver used is Serpent. In particular, a methodological physical approach for the error propagation analysis is presented and applied to the non-linear feedback loop of boron concentration, energy spectrum, cross-sections, flux and reaction rates, nuclide densities, and so forth.

The results indicate that employing average boron concentration may result in significant errors of 2% to 20% for the density and activity of the following nuclei of interest: Pd, Sm, Co, Rh, Eu, Ru, Np, Pu, and Am. These significant errors usually occur *during* the cycle and generally decrease over time, reaching negative values at EOC. This is explained by the major effect of flux errors, with values between 7.5 and −6%.

The results emphasize the benefits of high-fidelity models in assessing the radionuclide inventory in the core for the purpose of, for example, source term analysis. The results indicate that it is possible to employ the "best-estimate" calculation scheme with high accuracy rather than a conservative approach, in which, for example, the postulated inventory throughout the cycle is taken as the EOC inventory (worst case scenario). This work provides preliminary quantification of the accuracy of employing CBC, especially concerning the growing interest in high accuracy source term assessment and burnup credit analysis.

Finally, reactor shutdowns were simulated at different times during the cycle, and radionuclides densities were calculated for 100 days after shutdown. The analysis showed significant errors in the activity and radiotoxicity of the actinides, between 6% and −5%, mainly due to the error in neptunium buildup, which contributes to around 50% of the total actinides activity.

The investigation carried out in this work may constitute a starting point for future uncertainty and sensitivity analysis to study the influence of the spectrum variations (due to boron or other effects) on the source term calculation.

ACKNOWLEDGEMENTS

This research is funded by the Israeli Ministry of Energy, contract no. 219-11-115.

DATA AVAILABILITY STATEMENT

The data that support the findings of this study are available from the corresponding author upon reasonable request.

ORCID

Erez Gilad https://orcid.org/0000-0002-2130-9301

REFERENCES

1. Jutier L, Checiak B, Raby J, Aguiar L, Le Bars I. Conservative approach fo PWR MOX Burnup credit implementation. *Proceedings of the International Conference on the Physics of Reactors*. Switzerland: Paul Scherrer Institut - PSI; 2008.
2. Yehia H, Alcala-Ruiz F, Boado Magan HJ, et al. *Derivation of the Source Term and Analysis of the Radiological Consequences of Research Reactor Accidents*. Safety Report Series, No: International Atomic Energy Agency; 2008:53.
3. Castagna C, Cervi E, Lorenzi S, et al. A serpent/OpenFOAM coupling for 3D burnup analysis. *Eur Phys J Plus*. 2020;135(5):433-452.
4. Castagna C, Introini C, Cammi A. Development and implementation of a multi-physics high fidelity model of the TRIGA mark II reactor. *Ann Nucl Energy*. 2021;166:108704.
5. Wang J, Wang Q, Ding M. Review on neutronic/thermal-hydraulic coupling simulation methods for nuclear reactor analysis. *Ann Nucl Energy*. 2020;137:107165. Available from. doi:10.1016/j.anucene.2019.107165
6. Demazière C. *Modelling of Nuclear Reactor Multi-Physics*. London, United Kingdom: Academic Press; 2019.
7. Kochunas B, Collins B, Stimpson S, et al. VERA core simulator methodology for pressurized water reactor cycle depletion. *Nucl Sci Eng*. 2017;185(1):217-231.
8. Liu S, Liang J, Wu Q, et al. BEAVRS full core burnup calculation in hot full power condition by RMC code. *Ann Nucl Energy*. 2017;101:434-446.
9. Garcia M, Yurii B, et al. Validation of serpent-SUBCHANFLOW-TRANSURANUS pin-by-pin burnup calculations using experimental data from a pre-Konvoi PWR reactor. *Nucl Eng Des*. 2021;379:111173.
10. Cacuci DG. Handbook of nuclear engineering, Chap. 10. Springer; 2010.
11. NEA. 2011. Spent nuclear fuel assay data for isotopic validation - state of the art. Nuclear Energy Agency (NEA).
12. Leppänen J, Pusa M, Viitanen T, Valtavirta V, Kaltiaisenaho T. The serpent Monte Carlo code: status, development and applications in 2013. *Ann Nucl Energy*. 2015;82:142-150.
13. NuScale Power LLC. *NuScale Standard Plant Design Certification Application*. Portland, OR, United States: NuScale Power, LLC; 2020.
14. Reyes J, Ingersoll D. NuScale Power plant resilience studies. *Trans. Am. Nucl. Soc*. Philadelphia: PA; 2018 vol. 118.
15. Reyes J. NuScale plant safety in response to extreme events. *Nucl Technol*. 2012;178:153-163. Available from. doi:10.1080/00223131.2015.1038664
16. Pusa M, Leppänen J. Computing the matrix exponential in burnup caculations. *Nucl Sci Eng*. 2010;164(2):140-150.
17. Isotalo AE, Aarnio PA. Comparison of depletion algorithms for large systems of nuclides. *Ann Nucl Energy*. 2011;38(2):261-268. Available from: https://www.sciencedirect.com/science/article/pii/S0306454910003889
18. Bell GI, Glasstone S. *Nuclear reactor theory*. New York, United States: Van Nostrand Reinhold Company; 1970.
19. Isotalo A, Sahlberg V. Comparison of neutronics-depletion coupling schemes for burnup calculations. *Nucl Sci Eng*. 2015;179(4):434-459. Available from. doi:10.13182/NSE14-35
20. Ma Y, Liu S, Luo Z, et al. RMC/CTF multiphysics solutions to VERA core physics benchmark problem 9. *Ann Nucl Energy*. 2019;133:837-852.
21. Dufek J, Kotlyar D, Shwageraus E. The stochastic implicit Euler method - a stable coupling scheme for Monte Carlo burnup calculations. *Ann Nucl Energy*. 2013;60:295-300.
22. Chadwick MB, Herman M, Obložinský P, et al. ENDF/B-VII.1 nuclear data for science and technology: cross sections, Covariances, fission product yields and decay data. *Nucl Data Sheets*. 2011;112(12):2887-2996. Special Issue on ENDF/B-VII.1 Library. Available from: https://www.sciencedirect.com/science/article/pii/S009037521100113X
23. Ruggieri JM, Tommasi J, Lebrat JF, et al. ERANOS 2.1: International Code System for GEN IV Fast Reactor Analysis. In: Proceedings of ICAPP'06. American Nuclear Society ANS; 2006. .
24. Masterson RE. *Introduction to Nuclear Reactor Physics*. Boca Raton, FL, United States: CRC Press; 2018.
25. Soffer L, Burson SB, Ferrell CM, Lee RY, Ridgely JN. *Accident source terms for light-water nuclear power plants*. Washington, DC, United States: US Nuclear Regulatory Commission (NRC); 1995.
26. Mehboob K, Xinrong C, Ali M. Comprehensive review of source term analysis and experimental programs. *Res J Appl Sci Eng Technol*. 2012;4(17):3168-3181.
27. Rochman D, Leray O, Hursin M, et al. Nuclear data uncertainties for typical LWR fuel assemblies and a simple reactor Core. *Nucl Data Sheets*. 2017;139:1-76. Available from: https://www.sciencedirect.com/science/article/pii/S0090375217300017
28. Powers D, Leonard M, Gauntt R, Lee R, Salay M. *Accident source terms for light-water nuclear power plants using high-burnup or MOX fuel*. Albuquerque, New Mexico, United States: Sandia National Laboratories; 2011; SAND2011-0128.

How to cite this article: Castagna C, Gilad E. Study of radionuclide inventory in nuclear fuel under uncertainties in boron concentration using high-fidelity models. *Int J Energy Res*. 2022;1-13. doi:10.1002/er.7702